Particle hygroscopicity and its link to chemical composition in the urban atmosphere of Beijing, China during summertime

Z. J. Wu[1], J. Zheng[1], D. J. Shang[1], Z. F. Du[1], Y. S. Wu[1], L. M. Zeng[1], A. Wiedensohler[2], M. Hu[1]

[1] State Key Joint Laboratory of Environmental Simulation and Pollution Control, College of Environmental Sciences and Engineering, Peking University, Beijing 100871, China

[2] Leibniz Institute for Tropospheric Research, 04318, Leipzig, Germany

Corresponding to: Min Hu (minhu@pku.edu.cn) or Zhijun Wu (zhijunwu@pku.edu.cn)

Abstract:

Simultaneous measurements of particle number size distribution, particle hygroscopic properties, and size-resolved chemical composition were made during the summer of 2014 in Beijing, China. During the measurement period, the mean hygroscopicity parameters (κs) of 50, 100, 150, 200, and 250 nm particles were respectively 0.16±0.07, 0.19±0.06, 0.22±0.06, 0.26±0.07, and 0.28±0.10, showing an increasing trend with increasing particle size. Such size-dependency of particle hygroscopicity was similar to that of the inorganic mass fraction in PM_1. The hydrophilic mode (HGF>1.2) was more prominent in growth factor probability density distributions and its dominance of hydrophilic mode became more pronounced with increasing particle size. When $PM_{2.5}$ mass concentration is greater than 50 μg/m^3, the fractions of the hydrophilic mode for 150, 250, and 350 nm particles increased towards 1 as $PM_{2.5}$ mass concentration increased. This indicates that aged particles dominated during severe pollution periods in the atmosphere of Beijing. Particle hygroscopic growth can be well predicted using high time-resolution size-resolved chemical composition derived from AMS measurement using the ZSR mixing rule. The organic hygroscopicity parameter (κ_{org}) showed a positive correlation with oxygen to carbon ratio. During the new particle formation event associating with strongly active photochemistry, the hygroscopic growth factor or κ of newly formed particles is greater than for particle with the same sizes during non-NPF periods. A quick transformation from external mixture to internal mixture for pre-existing particles (for example 250 nm particle) was observed. Such

transformations may modify the state of mixture of pre-exiting particles and thus modify properties such as the light absorption coefficient and cloud condensation nuclei activation.

1 Introduction

Hygroscopic growth of atmospheric particles is one of the important parameters controlling their direct and indirect climate effects (McFiggans et al., 2006;Haywood and Boucher, 2000). Due to water uptake, hydrophilic particles grow significantly in size at high relative humidity (RH), which influences the particle light scattering and extinction coefficients, thereby impairing visibility (Sloane and Wolff, 1985). In addition, the water content of atmospheric aerosol particles can serve as a site for heterogeneous nucleation and reactions that perturb local photochemistry (Kreidenweis and Asa-Awuku, 2014). Therefore, a better understanding of hygroscopic behavior of atmospheric aerosol particle is required to further elucidate the physicochemical processes in the atmosphere.

The association of the particle chemical composition with their size-dependent hygroscopic behavior is rather complex. In order to overcome such complexities, Petters and Kreidenweis (2007) proposed a single hygroscopicity parameter (κ), namely κ-Köhler theory. On the basis of the κ-Köhler theory and Zdanovskii-Stokes-Robinson (ZSR) mixing rule (Stokes and Robinson, 1966;Zdanovskii, 1948), particle hygroscopic growth of a homogeneous chemical mixture can be predicted, knowing hygroscopic growth factors of pure chemical species. Aerosol mass spectrometers (AMS), which have been increasingly deployed in atmospheric aerosol studies, can provide a high time resolution of the size-resolved chemical composition of non-refractory particle material (DeCarlo et al., 2006). Therefore, coupled measurements of an AMS and a Hygroscopicity Tandem Differential Mobility Analyzer (H-TDMA) are able to capture highly variable changes in chemical particle composition and hygroscopicity in real time. Some studies highlighted the advantage of using size-selected AMS information over size-averaged

information from off-line chemical characterization (Medina et al., 2007;Gunthe et al., 2009;Cerully et al., 2011;Wu et al., 2013).

Another key product of AMS measurements is the oxidation level and chemical information of organic aerosols. Compared to inorganic species, which exhibit a well-characterized hygroscopic behavior, knowledge on the influence of the water uptake of the organic aerosols remains limited (Kanakidou et al., 2005;Hallquist et al., 2009). The hygroscopicity of organic material varies with its oxidation state (Jimenez et al., 2009), which may be highly variable in the real atmosphere, depending on the history of an air mass. Such variation may present a significant challenge when predicting hygroscopicity assuming a constant hygroscopic growth factor of the organic aerosol fraction at a given relative humidity, as has usually been done in closure studies.

Currently, some studies have been performed to investigate the relationship between particle hygroscopicity and chemical composition in both field measurements and laboratory experiments (Massoli et al., 2010;Wong et al., 2011;Lambe et al., 2011;Rickards et al., 2013;Moore et al., 2012b;Suda et al., 2014;Paramonov et al., 2013;Levin et al., 2012;Moore et al., 2012a). These works specially focused on parametrizing the empirical correlations between the atomic Oxygen : Carbon (O:C) ratio and organic hygroscopicity parameter (κ) derived from either hygroscopic growth factor (e.g. Wu et al., 2013;Rickards et al., 2013) or Cloud Condensation Nuclei (CCN) activity (e.g. Mei et al., 2013;Wong et al., 2011;Lambe et al., 2011;Chang et al., 2010). Typically, a linear parametrization of the correlation between κ and O:C was presented. Rickards et al. (2013) recently summarized the literature data and pointed out the systematic variability in parametrizations between organic κ and the O:C ratio determined from the different studies remains large. A recent work done by Suda et al. (2014) tested the influence of the number and location of molecular functional groups on the hygroscopicity of organic aerosols and may improve our understanding the mechanisms of organics hygroscopicity.

Over the past several decades, particle hygroscopicity measurements have been carried out world-wide, using the H-TDMA technique. Atmospheric environments, in

which those measurements were performed included marine, Antarctic, boreal forest, rural, and urban areas. Swietlicki et al. (2008) and Kreidenweis and Asa-Awu (2014) compiled the existing observations on particle hygroscopic growth in the literature. Throughout these compilations, measurements of particle hygroscopicity have been rarely performed in China, which is experiencing frequently severe haze pollution episodes. These few particle hygroscopicity measurements using the H-TDMA technique were deployed in Yangtze River Delta (Shanghai (Ye et al., 2013) and Hangzhou (Zhang et al., 2011)), Pearl River Delta (Xinken (Cheng et al., 2008) and Hong Kong (Lopez-Yglesias et al., 2014;Yeung et al., 2014)) and North China Plain (Beijing (Massling et al., 2009;Meier et al., 2009), Yufa (Achtert et al., 2009), and Wuqing (Liu et al., 2011)). Unfortunately, most of measurements lack a linkage between particle hygroscopicity and chemical composition with a high time resolution.

This study investigated the size-resolved particle hygroscopicity and chemical composition in Beijing, China, during summertime. Our work provided a general overview of particle hygroscopic behavior as well as a comparison of the observed hygroscopic particle growth and simulated one using AMS-based chemical particle composition, emphasizing on the organic mass fraction. Additionally, the evolution of particle hygroscopicity during the new particle formation event was investigated to understand the effects of strong photochemistry-driven atmospheric oxidation processes on particle hygroscopicity and the mixing state.

2 Measurements

2.1 The Sampling site

The sampling site is on the campus of Peking University, located in northwest Beijing. The laboratory was equipped with a suit of aerosol instruments sites on the roof of a building (30 m above the ground). The relative humidity (RH) of the sampled air was kept to below 30% using a silica gel dryer and a Nafion dryer in

series. The particle number size distribution, particle hygroscopicity, and aerosol mass spectrometric measurements were concurrently made. Particle number size distributions from 3 to 800 nm were measured by TSI-SMPS (Long-DMA3081+CPC3775 and Nano-DMA3085+UCPC3776). The multiple charge correction and particle loss correction were carried out. Other core instruments will be briefly described below.

2.2 Particle hygroscopicity measurements

The H-TDMA used in this study has been described in detail in previous publications (Wu et al., 2011;Massling et al., 2003), and complied to the instrumental standards and quality assurance prescribed in Massling et al. (2011). The H-TDMA consists of three main parts: (1) A Differential Mobility Analyzer (DMA1) that selects quasi-monodisperse particles, and a Condensation Particle Counter (CPC1) that measures the particle number concentration leaving the DMA1 at the selected particle size; (2) An aerosol humidifier conditioning the particles selected by DMA1 to a defined relative humidity (RH); (3) The second DMA (DMA2) coupled with another condensation particle counter (CPC2) to measure the number size distributions of the humidified particles. The second DMA and the aerosol humidification were placed in a temperature-controlled box. Hygroscopicity scans with 100 nm ammonium sulfate particles were performed every 3 hours to analyze the stability of the relative humidity of 90% in the second DMA. Hygroscopicity scan with a deviation of more than 3% in relative humidity to the set-point of 90% was not considered for further analysis.

The hygroscopic growth factor (*HGF*) is defined as the ratio of the particle mobility diameter, *Dp(RH)*, at a given RH to the dry diameter, Dp_{dry}:

$$\mathrm{HGF(RH)} = \frac{Dp(RH)}{Dp_{dry}} \qquad [1]$$

The TDMA*inv* method developed by Gysel et al. (2009) was used to invert the H-TDMA data. Dry scans (under RH<10%) were used to calibrate a possible offset between DMA1 and DMA2 and define the width of the H-TDMA's transfer function

(Gysel et al., 2009).

Based on the ZSR method , the *HGF* of a mixture can be estimated from the *HGFi* of the pure components and their respective volume fractions, εi (Malm and Kreidenweis, 1997):

$$HGF_{mixed} = (\sum_i \varepsilon_i HGF_i^3)^{1/3} \quad [2]$$

Here, we assumed that two components including soluble and insoluble fractions consist of aerosols (also refer to Ehn et al., 2007;Swietlicki et al., 1999). The soluble fraction was assumed to be ammonium sulfate. Then, the water-soluble volume fraction ($\varepsilon_{soluble}$) can be calculated by:

$$\varepsilon_{soluble} = \frac{HGF_{measured}^3 - 1}{HGF_{(NH4)_2SO_4}^3 - 1} \quad [3]$$

where $HGF_{measured}$ is the HGF of the particles measured by H-TDMA, and $HGF_{(NH4)2SO4}$ is the HGF of pure $(NH_4)_2SO_4$ particles with the same size. When calculating $HGF_{(NH4)2SO4}$ in different diameters, the parameterizations for $(NH_4)_2SO_4$ water activity developed by Potukuchi and Wexler (1995) and the density reported by Tang and Munkelwitz (1994) were used. The Kelvin term was considered in the calculation. In this study, the hygroscopic growth factors of 50, 100, 150, 250, and 350 nm particles were measured at RH=90%.

2.3 Particle chemical composition

The Aerodyne HR-ToF-AMS (here simply referred to as AMS) (DeCarlo et al., 2006) was operated with a time resolution of 5 minutes. Due to the 600˚C surface temperature of the vaporizer, the AMS can only analyze the non-refractory chemical composition of the particles. Elemental carbon, crustal material, and sea-salt cannot be detected. Therefore, based on the transmission efficiency of the aerodynamic lenses and the detected compounds, the AMS can provide the size-resolved chemical composition of the submicrometer non-refractory aerosol particle fraction ($NR\text{-}PM_1$) (Canagaratna et al., 2007). Applying the method developed by Canagarantna et al. (2015) the high resolution organic particle mass spectra were used to determine the elemental composition and the Oxygen to Carbon atomic ratio (O:C). The vacuum

aerodynamic diameter for AMS measurements was converted to the particle mobility diameter by division of AMS vacuum aerodynamic diameter by the estimated particle density (1500 kg/m^3). Here, the particle density is estimated by dividing the AMS-measured PM_1 and black carbon mass concentrations by the SMPS-derived particle volume concentration. Hereafter, the mobility diameter (assuming spherical particles) was used for AMS data below.

AMS-positive matrix factor (PMF) analysis was performed to identify different organic aerosols (OA) factors on the basis of the high resolution mass spectra of organics (Ulbrich et al., 2009). Four OA components were resolved by PMF, including low-volatility oxygenated organic aerosol (LV-OOA), semi-volatile oxygenated OA (SV-OOA), hydrocarbon-like OA (HOA) and cooking OA (COA). LV-OOA and SV-OOA typically represented aged SOA and freshly formed SOA, respectively (Ulbrich et al., 2009). HOA and COA were both anthropogenic primary organic aerosol (POA) components (Lanz et al., 2007).

Black carbon (BC) mass concentration in μg/m^3 is derived from Photoacoustic Extinctiometer (PAX) measurements (DMT Company) (Arnott et al., 1999) equipped with PM_1 cut-off inlet. In this study, PAX measurements were performed at wavelength 532 nm.

2.4 Meteorological parameters

Additionally, a weather station (Met One Instruments Inc.) provided the meteorological parameters. The wind speed, wind direction, ambient temperature, and relative humidity (RH) were detected.

Air mass backward trajectories arriving at the sampling site were calculated using the NOAA “HYSPLIT-4” (Hybrid Single-Particle Lagrangian Integrated Trajectory) model (Draxler and Hess, 1998). The 48 h trajectories terminated on a height of 200 m above the ground at 00:00, 06:00, 12:00 and 18:00 local time (UTC+08). In total, 100 air mass backward trajectories were grouped by assigning to five clusters using a k-means clustering algorithm. The number of clusters was

identified according to the changes of total spatial variance (TSV) (cf. HYSPLIT4 user's guide). Five was chosen as the final number of clusters considering optimum separation of trajectories (larger number of clusters) and simplicity of display (lower number of cluster).

3 Theory

3.1 Hygroscopicity parameter

The hygroscopicity parameter, κ, can be calculated from the hygroscopic growth factor (*HGF)* measured by H-TDMA (Petters and Kreidenweis, 2007):

$$\kappa_{HTDMA} = (HGF^3 - 1)\left(\frac{exp\left(\frac{A}{D_{Pdry} \cdot HGF}\right)}{RH} - 1\right) \quad [4]$$

$$A = \frac{4\sigma_{s/a} M_w}{RT\rho_w} \quad [5]$$

Where D_{Pdry} and *HGF* are the initial dry particle diameter and the hygroscopic growth factor at 90% RH measured by H-TDMA, respectively. $\sigma_{s/a}$ is the droplet surface tension (assumed to be that of pure water, $\sigma_{s/a}$ =0.0728 N m^{-2}), M_w the molecular weight of water, ρ_w the density of liquid water, R the universal gas constant, and T the absolute temperature.

For a given internal mixture, κ can also be predicted by a simple mixing rule on the basis of chemical volume fractions ε_i (Petters and Kreidenweis, 2007):

$$\kappa_{chem} = \sum_i \varepsilon_i \kappa_i \quad [6]$$

Here, κ_i and ε_i are the hygroscopicity parameters and volume fraction for the individual (dry) component in the mixture with *i* the number of components in the mixture. We derived ε_i from the particle chemical composition measured by AMS and PAX. The detailed description of how to calculate volume fraction is given in section 3.2. In the following discussions, κ_{HTDMA} and κ_{chem} denote respectively the values derived from H-TDMA and predicted using the ZSR mixing rule.

3.2 Hygroscopicity-chemical composition closure

The AMS provided the particle mass size distribution of sulfate (SO_4^{2-}), nitrate (NO_3^-), and ammonium (NH_4^+) ions as well that of organic compounds. We used a simplified ion pairing scheme as presented in Gysel et al. (2007) to convert the ion mass concentrations to the mass concentrations of their corresponding inorganic salts as listed in Table 1. Unlike inorganic salts, the hygroscopicity of organic aerosols is not well-recognized. In the literature, there were different approaches in representing κ_{org} in the closure studies. Typically, κ_{org} is assumed as a constant value. Chang et al., (2010) represented κ_{org} by using the factors from the PMF analysis to group organics measured by AMS into two components: a non-hygroscopic, unoxygenated component consisting of the hydrocarbon-like organic aerosol (HOA) factor and a hygroscopic component, consisting of the oxygenated factors LV-OOA, SV-OOA, and biomass burning organic aerosol (BBOA). In our study, organic materials derived from AMS measurements were grouped into two components including secondary organic aerosols (SOA) and primary organic aerosols (POA) based on AMS-PMF analysis. SOA, including LV-OOA and SV-OOA factors, is a more oxygenated organic aerosol, thereby more hygroscopic and has a κ_{SOA} of 0.1, which was calculated from the hygroscopic growth factor of organics at RH=90% as given in Gysel et al. (2007) using Eq. (4) in section 3.1. By taking κ_{SOA}=0.1, the best fit between κ_{HTDMA} and κ_{chem} was obtained in this study. One should note that kappa of SOA may varied with its oxidation state (Jimenez et al., 2009). The usage of a constant kappa value may introduce uncertainty in the closure of particle hygroscopicity and chemical composition. POA is the unoxygenated component consisting of the HOA and COA factors and is treated as hydrophobic material with κ_{POA} =0. Then, κ_{org} can be calculated as:

$$k_{org} = f_{POA} * k_{POA} + f_{SOA} * k_{SOA} \qquad [7]$$

Here, κ_{org} is overall κ for organic aerosols. f_{POA} and f_{SOA} are volume fraction of POA and SOA in total organic aerosols measured by AMS. One should note that Sun et al. (2012b) found that the contributions of POA and SOA to OA showed a

size-dependency. The relative contribution of POA to OA significantly increased with decreasing particle sizes. In this study, the closure studies were performed for particles with the mobility diameters of 150, 250, and 350 nm (larger than 200 nm in vacuum aerodynamic diameter). Using the relative contribution of POA to OA in PM_1 tended to overestimate percentage of POA for the size range focused in this study, thus underestimate the κ. In our case, the POA/OA and SOA/OA were respectively 0.39 and 0.61. According to equation [7], the κ_{org} can be calculated as 0.06 assuming κ_{SOA}=0.1. On the basis of Sun et al.'s study, the POA/OAs for 150, 250, and 350 nm particles were 0.30, 0.23, and 0.19, respectively. Using these ratios and equation [7], the calculated κ_{org}s were 0.07, 0.08, and 0.08, respectively, which were slightly higher than the one (κ_{org}=0.06) in our case. This minor difference can be negligible.

The volume fraction of each species was calculated from the particle mass concentration divided by its density as given in Table 1. The densities for inorganic salts were well defined. By summarizing the articles published (Park et al., 2004;McMurry et al., 2002;Kondo et al., 2011;Kiselev et al., 2010), 1700 kg/m^3 was selected as BC density. The hygroscopicity parameter κ of the hydrophobic black carbon was considered to be zero. The density of organic particle mass fraction including both SOA and POA was taken to be 1400 kg/m^3 (Gysel et al., 2007;Alfarra et al., 2006;Dinar et al., 2006). The κ_{HTDMA} values for the individual compounds listed in the Table 1 were calculated from the hygroscopic growth factor at 90% RH as given in Gysel et al. (2007) using equation [4] in the section 3.1.

4 Results and discussion

4.1 Meteorological condition during the sampling period

Fig. 1 showed the mean air mass backward trajectories for five clusters arriving at the sampling site from May 31 to June 24, 2014. The mean backward trajectories in five cluster showed the significant differences in direction and length. The air masses from the east (45%) and the south (26%) were the dominate trajectories. The

short-length air mass backward trajectories in cluster 1 and 2 indicated that air parcels moved slowly and spent much more time over the industrialized regions south and east of Beijing. As a result, the southerly and easterly air masses may be heavily polluted once they arrived at Beijing (Wehner et al., 2008). Cluster 3 spent much more time over the sea and may be associated with humid air masses. Northerly (8%) and north-westerly (10%) air masses, as represented by clusters 4–5, typically lead to the advection of dry and continental air into the Beijing area.

Fig. 2 displays the time series of wind speed, wind direction, ambient temperature, and RH during the sampling period. There was a clear diurnal cycle for all meteorological parameters. During nighttime, the wind speed was usually very low (around 1 m/s) and started to increase around noon on each day. The nighttime static wind may lead to very poor dilution with clean air and dispersion of pollutants and result in the local emissions were trapped in the urban atmosphere. The ambient temperature usually was above 30 ºC during daytime and around 20 ºC during nighttime. The average temperature and RH were respectively 24±7 °C and 45±20%. It rained several times during the measuring period, as indicated in the Fig. 2 (a). The heaviest wet deposition occurred on 17, June. The wet deposition obviously removed the atmospheric particles, as can be seen from the particle number size distribution shown in Fig. 3 (a).

In summer, the new particle formation and traffic emissions are the major sources of ultrafine particles in the atmosphere of Beijing (Wu et al., 2008;Wu et al., 2007). In addition, air masses across the industrialized regions in the south and east typically bring the high concentrations of accumulation mode particles to urban areas of Beijing (Wehner et al., 2008).

4.2 Overview of particle hygroscopic growth and the mixing state

Fig. 3 provides an overview of the particle number size distribution (a), hygroscopicity parameters (κ) (b), and chemical composition of PM_1 (c) during the entire field campaign. The trajectory clusters were marked as black circles in the Fig.

3 (a). As shown in the Fig. 3 (a), new particle formation (NPF) events were observed frequently. During the sampling period, the inorganic species and SOA were dominated in NR-PM_1 when air masses came from south and east of Beijing (trajectory cluster 1 and 2 as indicated by black circles in Fig.3 (a)). SOA was usually dominated in the organic compounds during the sampling period. Differently, the POA was a major fraction on June 7, 8, and 9, on which the BC mass fraction increased too. During this time period, the northerly air masses (trajectory cluster 5 marked in Fig. 3 (a)) arriving at the measurement site may be influenced by the wheat straw burning, which usually takes place from late May to early June over North China Plain. Several previous studies showed that wheat straw burning significantly contributes to degradation of air quality in Beijing during the harvest season in the summer (Li et al., 2008;Zheng et al., 2005).

Fig. 3 (b) displays the time series of hygroscopicity parameters for 50 nm (κ_{50nm}) and 250 nm (κ_{250nm}) particles. Both κ_{50nm} and κ_{250nm} had an obvious temporal variability. Their variations were similar to that of inorganic mass fraction in PM_1 displayed in Fig. 3 (c). An in-depth analysis of the relationship between particle hygroscopicity and chemical composition will be given in section 4.3. Fig. 4 gives an overview of growth factor probability density distributions (GF-PDF) for 50 and 250 nm particles during the entire field campaign. The GF-PDFs of both 50 and 250 nm showed two distinct modes, which are identified as hydrophobic mode (GF<1.2) and hydrophilic mode (GF>1.2). This implied that the particles were usually externally mixed. The hydrophilic mode of 250 nm particles is more prominent most of the time. Differently, the hydrophobic mode was dominated in 50 nm particles. As marked in the Fig. 4 (a) by the square with dashed line, the hydrophobic mode disappeared occasionally, indicating that the vast majority of particles in this size range can be fully hygroscopic. This phenomenon took place during the NPF events. A case study of particle hygroscopic behavior during the NPF event will be given in section 4.4.

Fig. 5 (left) shows the size-dependent particle hygroscopicity parameters and inorganic mass fraction of NR-PM_1 derived from averaging over the entire measuring period. The particle hygroscopicity increased with increasing particle size, displaying

the same size-dependency with the mass fraction of inorganic composition in NR-PM_1. This is because inorganics including ammonium sulfate and ammonium nitrate are major water-soluble chemical compounds in the atmospheric particles. Compared to inorganic components, the hygroscopicity parameter of organic aerosols are typically lower than 0.1 (Varutbangkul et al., 2006;Virkkula et al., 1999). The similar size-dependency of particle hygroscopicity was observed in various environments. For examples, Levin et al. (2012;2014) and Paramonov et al. (2013) reported that particle hygroscopicity increased with particle size at a forested site in Colorado and a boreal environment of southern Finland at the SMEAR station, respectively. Jurányi et al (2013) observed that particle hygroscopic growth increased with increasing dry diameter in the urban areas of Paris. Swietlicki et al. (2008) compiled worldwide H-TDMA data and found that the particle hgyroscopicity showed a pronounced size-dependency, with hygroscopicity increasing with particle diameter.

Fig. 5 (right) shows the size-dependency of the fraction of the hydrophilic mode. It can be seen that the hydrophilic mode was more prominent, no matter what particle size was considered. With increasing particle size, the dominance of hydrophilic mode became more pronounced. Above 150 nm, the number fraction of hydrophilic mode was around 0.8, and its size-dependency was insignificant. Below 150 nm, the number fraction of hydrophilic mode increases significantly with increasing particle size. The median number fraction of hydrophilic mode for 50 nm particles was 0.6, which was smaller than those of larger particles. Fors et al. (2011) also reported that smaller particles had a higher fraction of less hygroscopic particles in southern Sweden. Larger particles (here, above 150 nm) constituting a larger fraction of the hydrophilic mode can be explained as such: In the urban area, traffic emissions are major sources for particles below 100 nm. Typically, freshly emitted particles, such as soot, are initially hydrophobic and externally mixed. In contrast, larger particles have undergone atmospheric aging processes during transport (such as coagulation, condensation, chemical reaction) (Pöschl, 2005) for a longer time. These aging processes enhance the particle's water solubility (Pöschl, 2005;Jimenez et al., 2009) and result in more internally mixed particles.

Over the entire study, the mean κs of 50, 100, 150, 250, and 350 nm particles were 0.16±0.07, 0.19±0.06, 0.22±0.06, 0.26±0.07, and 0.28±0.10, respectively. These values were similar to the hygroscopicity parameter κ = 0.12-0.27 (measured at RH=90%) for 35–265 nm determined in the urban atmosphere of Paris (Jurányi et al., 2013). Yeung et al. (2014) observed that hygroscopicity κs of particles with sizes of 75, 100, 150, and 200 nm were respectively 0.28, 0.29, 0.26, and 0.27 when Hong Kong experienced a continental airstream. In their study, the particle hygroscopicity showed no obvious size-dependency and was higher than our observation in Beijing. In contrast, κs measured were relatively low at a forested site in Colorado (κ = 0.16±0.08 detected by CCNc), a boreal forest in Finland (κ = 0.18 at RH=90%) (Sihto et al., 2011), and a tropical forest site in the Amazon (κ = 0.16±0.06 detected by CCNc) (Gunthe et al., 2009). At these forested locations, organic species were predominance in particles. Differently, in the atmosphere of Beijing, the inorganic fraction was relatively dominated, as shown in the Fig.3 (c).

The haze issue caused by high aerosol loadings over the northern plain of China is a major concern, for both air quality and climate effects. Here, the $PM_{2.5}$ mass concentration which measured by TEOM$^{@}$ Monitor (Series 1400ab), a key factor characterizing air pollution, vs. the fraction of the hydrophilic mode is plotted (Fig. 6) to analyze the relationship between the particle mixing state and air pollution. There was no obvious dependency between the $PM_{2.5}$ mass concentration and the number fraction of hydrophilic mode for 50 nm particles, which can be expected due to the low mass fraction of ultrafine particles. This was however also true for 150, 250, and 350 nm particles, if $PM_{2.5}$ mass concentration is lower than 50 μg/m^3. The reason for this is that the particle mass concentration is dominated by local sources and less by secondary aerosol particles formed during long-range transport. Conversely, when $PM_{2.5}$ mass concentration was larger than 50 μg/m^3, the fraction of the hydrophilic mode was larger than 0.7. With the increasing $PM_{2.5}$ mass concentration, the fraction rose towards to 1, indicating that the aged aerosols were dominant. This means that secondary aerosol particles were dominant during severe particulate pollution episodes, occurring frequently in Beijing. Our results were consistent to recent

scientific findings (Guo et al., 2014;Huang et al., 2014), which pointed out that the haze pollution events were mainly attributable to secondary aerosol formation.

4.3 Closure between particle hygroscopicity and chemical components

The AMS-derived particle mass concentrations for different chemical compounds were used to perform a closure study. The particle mass concentrations for individual species were integrated over the size interval of D_{Pdry}±50 nm. Here, D_{Pdry} is the dry particle diameter selected by H-TDMA. Considering the limited signal statistics in this narrow size range, AMS data were used to carry out the closure only if the sum of sulfate, nitrate, ammonium, and organics mass concentrations derived from integrating size range of D_{Pdry}±50 nm was greater than 1 $\mu g/m^3$.

The BC particle mass concentration within the size range of D_{Pdry} ±50 nm was estimated as follows: First, the ratio ($R_{BC/PM1}$) of BC particle mass concentration (derived from PAX) to bulk particle mass concentration (derived from AMS measurement) was calculated, assuming this ratio was independent on the particle size. Afterwards, the BC particle mass concentration in a certain size range, e.g., 150±50 nm was estimated by multiplying the mass concentration derived from integrating particle size range of 150±50 nm (AMS data) and $R_{BC/PM1}$. One should note that this assumption may give an uncertainty in the closure, because the BC mass concentration has a dependency with particle size (Huang et al., 2006). Sun et al. (2012a) reported that the average mass size distribution of BC had one mode peaking at a volume-equivalent diameter of 207 nm. The sizes of 150, 250, 350 nm covered the peak of BC mass size distribution. As a result, the BC mass concentration for particles in diameter of 150, 250, and 350 nm should be higher than that estimated with the assumption of uniformly distributed BC across the whole particle size range.

The SOA and POA mass fractions within the size range of D_{Pdry} ±50 nm were estimated using a similar method as the calculation of BC mass concentration given above. The POA (MF_{POA}) and SOA (MF_{SOA}) mass fractions in total organic aerosols in NR-PM1 are calculated on a basis of the AMS-PMF analysis results. Assuming

MF_{POA} and MF_{SOA} were independent of the particle diameter, the POA or SOA mass concentration in the size range D_{Pdry}±50 nm can be calculated by multiplying the organic mass concentration derived from integrating particle size range of 150±50 nm (AMS data) and MF_{POA} or MF_{SOA}. Fig. 7 shows the scattering plots of κ_{chem} calculated from the size-resolved chemical composition against κ_{HTDMA}. The fitted slopes for 150, 250, and 350 nm particles were 1.02, 0.99, and 0.97, respectively, which is close to unit. The root mean square errors (RMSE) of these linear fits were 0.04. This indicates that the measured κ can be well predicted on a basis of AMS data and the ZSR mixing rule. While, one should note that the assumption of BC mass size distribution and κ_{org} value in the closure as well as the measurement uncertainties for both H-TDMA and AMS could introduce the biases in the closure. This may lead to a scatter of data point around the fitting line.

Assuming the inorganic fraction was fully explained by the ZSR mixing rule, κ_{org} can be calculated by subtracting κ of inorganic fraction and BC from κ_{HTDMA}. Here, κ_{org} for 150 nm particles was calculated because it provided a better closure result and higher organic fraction in contrast to other particle sizes. Duplissy et al. (2011) pointed out that the uncertainty in the estimation of κ_{org} decreases with increasing organic fraction, thereby, only data featuring organic fractions larger than 50% were used in this calculation. In addition, the evaporation of NH_4NO_3 could occur in the DMAs and the humidification section. This leads to a positive prediction bias because the volatile NH_4NO_3, which is fully detected by AMS, can evaporate in the H-TDMA system (Gysel et al., 2007). Here, only data with NH_4NO_3 volume fraction below 20% were considered in order to reduce the evaporation artifact of NH_4NO_3. Restricting data to times when ammonium nitrate is below 20% and organics were greater than 50% may lead to a bias in data points between daytime and nighttime. The statistics showed that nighttime data points (204 data points) were more than those during daytime (160 data points). This is because that the organic mass fraction during nighttime was higher than that during daytime. This bias could make the fit between κ_{org} and O:C ratio more representative for nighttime situation than daytime.

Fig. 8 shows κ_{org} as a function of O:C ratio. From the degree of scatter point of view, κ_{org} was not correlated to the O:C ratio. Several previous studies reported the similar plots of κ_{org} values as a function of O:C ratios (Chang et al., 2010;Bhattu and Tripathi, 2015;Rickards et al., 2013). In order to derive an empirical relationship between κ_{org} and O:C ratios, κ_{org} values were usually binned by O:C in increments of 0.1. As displayed in Fig. 8, a linear fitting function (κ_{org}=(0.08±0.02)*O:C+(0.02±0.01)) was obtained. Some empirical functions reported by other previous studies were also shown in Fig.8. In these previous studies (Wu et al., 2013;Jimenez et al., 2009;Rickards et al., 2013;Duplissy et al., 2011), the κ_{org} were derived from the measurements performed in the sub-saturation regime. In Massoli et al.' study (2010) (not shown in the Fig. 8 due to the linear fitting using HGF, not κ_{org}) ,they reported a linear relationship ($HGF_{90\%}$ = (0.58±0.15)*O:C + (0.85 ± 0.08)) between $HGF_{90\%}$ and O:C for the laboratory-generated SOA particles. Both results displayed in Fig. 8 and Massoli's study showed a positive correlation between κ_{org} and O:C. Such positive correlation was also reported by those studies based on CCNc measurements, for examples, Chang et al. (2010) and Mei et al. (2013). We note that the slopes of the linear fitting varied with different studies, indicating there was no a simple parametrization to describe the relationship between organic hygroscopicity and its oxidation state though the various atmospheric environments. Recently, Richards et al. (2013) had undertaken an extensive review of κ values published in the literature and showed that κ_{org} vs. O:C plot has a large degree of scatter. This indicates that other factors, such as phase state (Pajunoja et al., 2015) and molecular structures (Suda et al., 2014) of organic aerosols (OA) other than oxidation state may also play a role in the determination of the OA hygroscopicity.

4.4 Case study: particle hygroscopicity during a NPF event

As shown in Fig. 3 (a), the NPF events frequently took place during the sampling period. In order to understand the effects of NPF on particle hygroscopic behavior, this section will exemplify the evolution of particle hygroscopicity during a NPF

event. As an example, Fig. 9 displays the time series of particle number size distribution, GF-PDFs and water soluble fraction of 50 and 250 nm particles, and chemical composition of PM_1 during a NPF event occurred on 5th June, 2014. Here, the particles with 50 nm in diameter represented the newly formed particles, and particles with 250 nm in diameter represented the pre-existing particles.

The NPF event started at around 10:30 am and ended at 5:30 am the next day. After the starting of new particle formation, the number fraction of the hydrophilic mode for 50 nm particles increased from 0.5 to around 1, showing the conversion of externally to more internally mixed particles, as marked by the black dashed lines in Fig. 9 (b). Around 8:30 pm, the fraction of the hydrophilic mode particles dropped to 0.6, and the hydrophobic mode appeared again. This is attributed to the intensive traffic emissions at the time of rush hour, which can clearly be seen from the particle number size distribution. During nighttime, the growth factor of hydrophilic mode particles decreased. This can be explained by sulfuric acid condensation playing a minor role in particle growth during nighttime. Simultaneously, ambient temperature decreased from 27 to 20 ˚C. Lower temperature facilitated the condensation of semi-volatile organic vapors onto the newly formed particles. The chemical composition of PM1 also (Fig. 9 (d)) showed that the inorganic species and SOA were dominated before 8:30 pm, while mass fraction of organic compounds, especially POA increased significantly afterwards.

Clearly, an obvious enhancement in the water soluble fraction of 50 nm particles took place after the NPF event started. Similar phenomenon was also observed by Shantz et al. (2012), which showed that the 36 nm particles became increasingly CCN active within 1-4 h after the nucleation during the NPF events. They hypothesized that the condensation of sulphate on these small particles enhanced their CCN activity. The water soluble fraction accounted for 42% in 50 nm newly formed particles. The water soluble fraction was most likely ammonium sulfate formed from neutralization reaction between ammonia and sulfuric acid. In contrast, the newly formed particles consisted a minor fraction of water soluble fraction (16%) in Hyytiälä, Finland (Ehn et al., 2007). Other observations in the clean atmospheric environments (relative to

Beijing), such as a forested site in Colorado (Levin et al., 2012), Mace Head, Ireland (Väkevä et al., 2002), Melpitz, Germany (Wu et al., 2015) also showed that low water soluble compounds, most likely secondary organic species mainly contributed to new particle growth. Differently, in urban Atlanta (Sakurai et al., 2005), the water soluble fraction was dominated in the newly formed particles, which was similar to our observation in this study.

As shown in Figure 9 (c), the fraction of the hydrophilic mode of 250 nm particles increased significantly and approached 1 after the NPF event started. This can be explained as such: during the particle formation, a large amount of condensable vapors, such as sulfuric acid and secondary organic species produced because of the strongly active photochemistry. These condensable vapors can condense onto the pre-existing particle and result in the transformation of external mixture to internal mixture. Such transformation may alter the atmospheric behaviors of pre-exiting particles, such as optical property and cloud condensation nuclei activation during the new particle formation events.

5 Conclusions

Particle number size distribution, particle hygroscopicity, and size-resolved chemical composition were measured concurrently during summertime 2014 in Beijing, China. The particle hygroscopicity showed a pronounced size-dependency. It increased with increasing particle size. During the measurement period, the mean κs of 50, 100, 150, 200, and 250 nm particles are 0.16±0.07, 0.19±0.06, 0.22±0.06, 0.26±0.07, and 0.28±0.10, respectively. The size-dependency behavior of particle hygroscopicity was similar to that of inorganic compounds in PM_1. The hydrophilic mode (HGF>1.2) was more prominent, no matter what particle size was considered. With increasing particle size, the dominance of hydrophilic mode became more pronounced. When $PM_{2.5}$ mass concentration was below 50μg/m^3, no dependency between $PM_{2.5}$ mass concentration and the number fraction of hydrophilic mode was found. Above 50 μg/m^3, the number fraction of hydrophilic mode for 150, 250, 350

nm particles increased and rose towards to 1 with the increasing $PM_{2.5}$ mass concentration. This means that aged particles was dominated the particle mass concentration, especially during severe particulate pollution events in Beijing. Based on the size-resolved AMS data, the particle hygroscopic growth can be well predicted using the ZSR method. The organic hygroscopicity parameter showed a positive correlation with O:C ratio.

Frequent new particle formation events took place during the measuring period. The hygroscopic growth factor or κ of newly formed particles was greater than the hygroscopic growth factor of particles with the same sizes during non-NPF periods. During the new particle formation, fast transformations of external mixture to internal mixture for existing particles (for example 250 nm particle) have been observed. This was a strong indication that secondary aerosol material such as organics and sulfates were produced due to the strongly active photochemistry during NPF events, and subsequently condensed onto the particles. Such transformation may modify the atmospheric behaviors of pre-exiting particles, such as optical property and cloud condensation nuclei activation.

Acknowledgement

This work is supported by the following projects: National Natural Science Foundation of China (41475127), National Basic Research Program of China (2013CB228503), and Special Fund of State Key Joint Laboratory of Environment Simulation and Pollution Control (14L02ESPC). The authors would like to thank Douglas R. Worsnop for useful discussion about the AMS size distribution data processing.

Reference

Achtert, P., Birmili, W., Nowak, A., Wehner, B., Wiedensohler, A., Takegawa, N., Kondo, Y., Miyazaki, Y., Hu, M., and Zhu, T.: Hygroscopic growth of tropospheric particle number size distributions over the North China Plain, Journal of Geophysical Research: Atmospheres, 114, n/a-n/a, 10.1029/2008JD010921, 2009.

Alfarra, M. R., Paulsen, D., Gysel, M., Garforth, A. A., Dommen, J., Prévôt, A. S. H., Worsnop, D. R., Baltensperger, U., and Coe, H.: A mass spectrometric study of secondary organic aerosols formed from the photooxidation of anthropogenic and biogenic precursors in a reaction chamber, Atmos. Chem. Phys., 6, 5279-5293, 10.5194/acp-6-5279-2006, 2006.

Arnott, P., Moosmüller, H., Fred Rogers, C., Jin, T., and Bruch, R.: Photoacoustic spectrometer for measuring light absorption by aerosol: instrument description, Atmospheric Environment, 33, 2845-2852, http://dx.doi.org/10.1016/S1352-2310(98)00361-6, 1999.

Bhattu, D., and Tripathi, S. N.: CCN closure study: Effects of aerosol chemical composition and mixing state, Journal of Geophysical Research: Atmospheres, 120, 2014JD021978, 10.1002/2014JD021978, 2015.

Canagaratna, M. R., Jayne, J. T., Jimenez, J. L., Allan, J. D., Alfarra, M. R., Zhang, Q., Onasch, T. B., Drewnick, F., Coe, H., Middlebrook, A., Delia, A., Williams, L. R., Trimborn, A. M., Northway, M. J., DeCarlo, P. F., Kolb, C. E., Davidovits, P., and Worsnop, D. R.: Chemical and microphysical characterization of ambient aerosols with the aerodyne aerosol mass spectrometer, Mass Spectrometry Reviews, 26, 185-222, 10.1002/mas.20115, 2007.

Canagaratna, M. R., Jimenez, J. L., Kroll, J. H., Chen, Q., Kessler, S. H., Massoli, P., Hildebrandt Ruiz, L., Fortner, E., Williams, L. R., Wilson, K. R., Surratt, J. D., Donahue, N. M., Jayne, J. T., and Worsnop, D. R.: Elemental ratio measurements of organic compounds using aerosol mass spectrometry: characterization, improved calibration, and implications, Atmos. Chem. Phys., 15, 253-272, 10.5194/acp-15-253-2015, 2015.

Cerully, K. M., Raatikainen, T., Lance, S., Tkacik, D., Tiitta, P., Petäjä, T., Ehn, M., Kulmala, M., Worsnop, D. R., Laaksonen, A., Smith, J. N., and Nenes, A.: Aerosol hygroscopicity and CCN activation kinetics in a boreal forest environment during the 2007 EUCAARI campaign, Atmos. Chem. Phys., 11, 12369-12386, 10.5194/acp-11-12369-2011, 2011.

Chang, R. Y. W., Slowik, J. G., Shantz, N. C., Vlasenko, A., Liggio, J., Sjostedt, S. J., Leaitch, W. R., and Abbatt, J. P. D.: The hygroscopicity parameter (κ) of ambient organic aerosol at a field site subject to biogenic and anthropogenic influences: relationship to degree of aerosol oxidation, Atmos. Chem. Phys., 10, 5047-5064, 10.5194/acp-10-5047-2010, 2010.

Cheng, Y. F., Wiedensohler, A., Eichler, H., Heintzenberg, J., Tesche, M., Ansmann, A., Wendisch, M., Su, H., Althausen, D., Herrmann, H., Gnauk, T., Brüggemann, E., Hu, M., and Zhang, Y. H.: Relative humidity dependence of aerosol optical properties and direct radiative forcing in the surface boundary layer at Xinken in Pearl River Delta of China: An observation based numerical study, Atmospheric Environment, 42, 6373-6397, http://dx.doi.org/10.1016/j.atmosenv.2008.04.009, 2008.

DeCarlo, P. F., Kimmel, J. R., Trimborn, A., Northway, M. J., Jayne, J. T., Aiken, A. C., Gonin, M., Fuhrer, K., Horvath, T., Docherty, K. S., Worsnop, D. R., and Jimenez, J. L.: Field-Deployable, High-Resolution, Time-of-Flight Aerosol Mass Spectrometer, Analytical Chemistry, 78, 8281-8289, 10.1021/ac061249n, 2006.

Dinar, E., Mentel, T. F., and Rudich, Y.: The density of humic acids and humic like substances (HULIS) from fresh and aged wood burning and pollution aerosol particles, Atmos. Chem. Phys., 6, 5213-5224, 10.5194/acp-6-5213-2006, 2006.

Draxler, R. R., and Hess, G. D.: An overview of the HYSPLIT_4 modelling system for trajectories dispersion and deposition, Australian Meteorological Magazine, 47, 295-308, 1998.

Duplissy, J., DeCarlo, P. F., Dommen, J., Alfarra, M. R., Metzger, A., Barmpadimos, I., Prevot, A. S. H., Weingartner, E., Tritscher, T., Gysel, M., Aiken, A. C., Jimenez, J. L., Canagaratna, M. R., Worsnop, D. R., Collins, D. R., Tomlinson, J., and Baltensperger, U.: Relating hygroscopicity and composition of organic aerosol particulate matter, Atmos. Chem. Phys., 11, 1155-1165, 10.5194/acp-11-1155-2011, 2011.

Ehn, M., Petäjä, T., Aufmhoff, H., Aalto, P., Hämeri, K., Arnold, F., Laaksonen, A., and Kulmala, M.: Hygroscopic properties of ultrafine aerosol particles in the boreal forest: diurnal variation, solubility and the influence of sulfuric acid, Atmos. Chem. Phys., 7, 211-222, 10.5194/acp-7-211-2007, 2007.

Fors, E. O., Swietlicki, E., Svenningsson, B., Kristensson, A., Frank, G. P., and Sporre, M.: Hygroscopic properties of the ambient aerosol in southern Sweden – a two year study, Atmos. Chem. Phys., 11, 8343-8361, 10.5194/acp-11-8343-2011, 2011.

Gunthe, S. S., King, S. M., Rose, D., Chen, Q., Roldin, P., Farmer, D. K., Jimenez, J. L., Artaxo, P., Andreae, M. O., Martin, S. T., and Pöschl, U.: Cloud condensation nuclei in pristine tropical rainforest air of Amazonia: size-resolved measurements and modeling of atmospheric aerosol composition and CCN activity, Atmos. Chem. Phys., 9, 7551-7575, 10.5194/acp-9-7551-2009, 2009.

Guo, S., Hu, M., Zamora, M. L., Peng, J., Shang, D., Zheng, J., Du, Z., Wu, Z., Shao, M., Zeng, L., Molina, M. J., and Zhang, R.: Elucidating severe urban haze formation in China, Proceedings of the National Academy of Sciences, 111, 17373-17378, 10.1073/pnas.1419604111, 2014.

Gysel, M., Crosier, J., Topping, D. O., Whitehead, J. D., Bower, K. N., Cubison, M. J., Williams, P. I., Flynn, M. J., McFiggans, G. B., and Coe, H.: Closure study between chemical composition and hygroscopic growth of aerosol particles during TORCH2, Atmos. Chem. Phys., 7, 6131-6144, 10.5194/acp-7-6131-2007, 2007.

Gysel, M., McFiggans, G. B., and Coe, H.: Inversion of tandem differential mobility analyser (TDMA) measurements, Journal of Aerosol Science, 40, 134-151, 10.1016/j.jaerosci.2008.07.013, 2009.

Hallquist, M., Wenger, J. C., Baltensperger, U., Rudich, Y., Simpson, D., Claeys, M., Dommen, J., Donahue, N. M., George, C., Goldstein, A. H., Hamilton, J. F., Herrmann, H., Hoffmann, T., Iinuma, Y., Jang, M., Jenkin, M. E., Jimenez, J. L., Kiendler-Scharr, A.,

Maenhaut, W., McFiggans, G., Mentel, T. F., Monod, A., Prevot, A. S. H., Seinfeld, J. H., Surratt, J. D., Szmigielski, R., and Wildt, J.: The formation, properties and impact of secondary organic aerosol: current and emerging issues, Atmospheric Chemistry and Physics, 9, 5155-5236, 2009.

Haywood, J., and Boucher, O.: Estimates of the direct and indirect radiative forcing due to tropospheric aerosols: A review, Reviews of Geophysics, 38, 513-543, 10.1029/1999RG000078, 2000.

Huang, R.-J., Zhang, Y., Bozzetti, C., Ho, K.-F., Cao, J.-J., Han, Y., Daellenbach, K. R., Slowik, J. G., Platt, S. M., Canonaco, F., Zotter, P., Wolf, R., Pieber, S. M., Bruns, E. A., Crippa, M., Ciarelli, G., Piazzalunga, A., Schwikowski, M., Abbaszade, G., Schnelle-Kreis, J., Zimmermann, R., An, Z., Szidat, S., Baltensperger, U., Haddad, I. E., and Prevot, A. S. H.: High secondary aerosol contribution to particulate pollution during haze events in China, Nature, 514, 218-222, 10.1038/nature13774 http://www.nature.com/nature/journal/v514/n7521/abs/nature13774.html#supplementary-information, 2014.

Huang, X. F., Yu, J. Z., He, L. Y., and Hu, M.: Size distribution characteristics of elemental carbon emitted from Chinese vehicles: Results of a tunnel study and atmospheric implications, Environmental Science & Technology, 40, 5355-5360, 10.1021/es0607281, 2006.

Jimenez, J. L., Canagaratna, M. R., Donahue, N. M., Prevot, A. S. H., Zhang, Q., Kroll, J. H., DeCarlo, P. F., Allan, J. D., Coe, H., Ng, N. L., Aiken, A. C., Docherty, K. S., Ulbrich, I. M., Grieshop, A. P., Robinson, A. L., Duplissy, J., Smith, J. D., Wilson, K. R., Lanz, V. A., Hueglin, C., Sun, Y. L., Tian, J., Laaksonen, A., Raatikainen, T., Rautiainen, J., Vaattovaara, P., Ehn, M., Kulmala, M., Tomlinson, J. M., Collins, D. R., Cubison, M. J., E, Dunlea, J., Huffman, J. A., Onasch, T. B., Alfarra, M. R., Williams, P. I., Bower, K., Kondo, Y., Schneider, J., Drewnick, F., Borrmann, S., Weimer, S., Demerjian, K., Salcedo, D., Cottrell, L., Griffin, R., Takami, A., Miyoshi, T., Hatakeyama, S., Shimono, A., Sun, J. Y., Zhang, Y. M., Dzepina, K., Kimmel, J. R., Sueper, D., Jayne, J. T., Herndon, S. C., Trimborn, A. M., Williams, L. R., Wood, E. C., Middlebrook, A. M., Kolb, C. E., Baltensperger, U., and Worsnop, D. R.: Evolution of organic aerosols in the atmosphere, Science, 326, 1525-1529, 10.1126/science.1180353, 2009.

Jurányi, Z., Tritscher, T., Gysel, M., Laborde, M., Gomes, L., Roberts, G., Baltensperger, U., and Weingartner, E.: Hygroscopic mixing state of urban aerosol derived from size-resolved cloud condensation nuclei measurements during the MEGAPOLI campaign in Paris, Atmos. Chem. Phys., 13, 6431-6446, 10.5194/acp-13-6431-2013, 2013.

Kanakidou, M., Seinfeld, J. H., Pandis, S. N., Barnes, I., Dentener, F. J., Facchini, M. C., Van Dingenen, R., Ervens, B., Nenes, A., Nielsen, C. J., Swietlicki, E., Putaud, J. P., Balkanski, Y., Fuzzi, S., Horth, J., Moortgat, G. K., Winterhalter, R., Myhre, C. E. L., Tsigaridis, K., Vignati, E., Stephanou, E. G., and Wilson, J.: Organic aerosol and global climate modelling: a review, Atmospheric Chemistry and Physics, 5, 1053-1123, 2005.

Kiselev, A., Wennrich, C., Stratmann, F., Wex, H., Henning, S., Mentel, T. F., Kiendler-Scharr, A., Schneider, J., Walter, S., and Lieberwirth, I.: Morphological characterization of soot aerosol particles during LACIS Experiment in November (LExNo), Journal of Geophysical Research-Atmospheres, 115, Artn D11204
Doi 10.1029/2009jd012635, 2010.

Kondo, Y., Sahu, L., Moteki, N., Khan, F., Takegawa, N., Liu, X., Koike, M., and Miyakawa, T.: Consistency and Traceability of Black Carbon Measurements Made by Laser-Induced Incandescence, Thermal-Optical Transmittance, and Filter-Based Photo-Absorption Techniques, Aerosol Science and Technology, 45, 295-312, 10.1080/02786826.2010.533215, 2011.

Kreidenweis, S. M., and Asa-Awuku, A.: 5.13 - Aerosol Hygroscopicity: Particle Water Content and Its Role in Atmospheric Processes, in: Treatise on Geochemistry (Second Edition), edited by: Turekian, H. D. H. K., Elsevier, Oxford, 331-361, 2014.

Lambe, A. T., Onasch, T. B., Massoli, P., Croasdale, D. R., Wright, J. P., Ahern, A. T., Williams, L. R., Worsnop, D. R., Brune, W. H., and Davidovits, P.: Laboratory studies of the chemical composition and cloud condensation nuclei (CCN) activity of secondary organic aerosol (SOA) and oxidized primary organic aerosol (OPOA), Atmos. Chem. Phys., 11, 8913-8928, 10.5194/acp-11-8913-2011, 2011.

Lanz, V. A., Alfarra, M. R., Baltensperger, U., Buchmann, B., Hueglin, C., and Prévôt, A. S. H.: Source apportionment of submicron organic aerosols at an urban site by factor analytical modelling of aerosol mass spectra, Atmos. Chem. Phys., 7, 1503-1522, 10.5194/acp-7-1503-2007, 2007.

Levin, E. J. T., Prenni, A. J., Petters, M. D., Kreidenweis, S. M., Sullivan, R. C., Atwood, S. A., Ortega, J., DeMott, P. J., and Smith, J. N.: An annual cycle of size-resolved aerosol hygroscopicity at a forested site in Colorado, J. Geophys. Res., 117, D06201, 10.1029/2011jd016854, 2012.

Levin, E. J. T., Prenni, A. J., Palm, B. B., Day, D. A., Campuzano-Jost, P., Winkler, P. M., Kreidenweis, S. M., DeMott, P. J., Jimenez, J. L., and Smith, J. N.: Size-resolved aerosol composition and its link to hygroscopicity at a forested site in Colorado, Atmos. Chem. Phys., 14, 2657-2667, 10.5194/acp-14-2657-2014, 2014.

Li, L., Wang, Y., Zhang, Q., Li, J., Yang, X., and Jin, J.:
Wheat straw burning and its associated impacts on Beijing air quality, Science in China Series D: Earth Sciences, 51, 403-414, 2008.

Liu, P. F., Zhao, C. S., Göbel, T., Hallbauer, E., Nowak, A., Ran, L., Xu, W. Y., Deng, Z. Z., Ma, N., Mildenberger, K., Henning, S., Stratmann, F., and Wiedensohler, A.: Hygroscopic properties of aerosol particles at high relative humidity and their diurnal variations in the North China Plain, Atmos. Chem. Phys., 11, 3479-3494, 10.5194/acp-11-3479-2011, 2011.

Lopez-Yglesias, X. F., Yeung, M. C., Dey, S. E., Brechtel, F. J., and Chan, C. K.: Performance Evaluation of the Brechtel Mfg. Humidified Tandem Differential Mobility Analyzer (BMI HTDMA) for Studying Hygroscopic Properties of Aerosol Particles, Aerosol Science and Technology, 48, 969-980, 10.1080/02786826.2014.952366, 2014.

Malm, W. C., and Kreidenweis, S. M.: The effects of models of aerosol hygroscopicity on the apportionment of extinction, Atmospheric Environment, 31, 1965-1976, 10.1016/s1352-2310(96)00355-x, 1997.

Massling, A., Wiedensohler, A., Busch, B., Neusüß, C., Quinn, P., Bates, T., and Covert, D.: Hygroscopic properties of different aerosol types over the Atlantic and Indian Oceans, Atmos. Chem. Phys., 3, 1377-1397, 10.5194/acp-3-1377-2003, 2003.

Massling, A., Stock, M., Wehner, B., Wu, Z. J., Hu, M., Brüggemann, E., Gnauk, T., Herrmann, H., and Wiedensohler, A.: Size segregated water uptake of the urban submicrometer aerosol in Beijing, Atmospheric Environment, 43, 1578-1589, http://dx.doi.org/10.1016/j.atmosenv.2008.06.003, 2009.

Massling, A., Niedermeier, N., Hennig, T., Fors, E. O., Swietlicki, E., Ehn, M., Hämeri, K., Villani, P., Laj, P., Good, N., McFiggans, G., and Wiedensohler, A.: Results and recommendations from an intercomparison of six Hygroscopicity-TDMA systems, Atmos. Meas. Tech., 4, 485-497, 10.5194/amt-4-485-2011, 2011.

Massoli, P., Lambe, A. T., Ahern, A. T., Williams, L. R., Ehn, M., Mikkilä, J., Canagaratna, M. R., Brune, W. H., Onasch, T. B., Jayne, J. T., Petäjä, T., Kulmala, M., Laaksonen, A., Kolb, C. E., Davidovits, P., and Worsnop, D. R.: Relationship between aerosol oxidation level and hygroscopic properties of laboratory generated secondary organic aerosol (SOA) particles, Geophysical Research Letters, 37, n/a-n/a, 10.1029/2010GL045258, 2010.

McFiggans, G., Artaxo, P., Baltensperger, U., Coe, H., Facchini, M. C., Feingold, G., Fuzzi, S., Gysel, M., Laaksonen, A., Lohmann, U., Mentel, T. F., Murphy, D. M., O'Dowd, C. D., Snider, J. R., and Weingartner, E.: The effect of physical and chemical aerosol properties on warm cloud droplet activation, Atmospheric Chemistry and Physics, 6, 2593-2649, 2006.

McMurry, P. H., Wang, X., Park, K., and Ehara, K.: The Relationship between Mass and Mobility for Atmospheric Particles: A New Technique for Measuring Particle Density, Aerosol Science and Technology, 36, 227-238, 10.1080/027868202753504083, 2002.

Medina, J., Nenes, A., Sotiropoulou, R.-E. P., Cottrell, L. D., Ziemba, L. D., Beckman, P. J., and Griffin, R. J.: Cloud condensation nuclei closure during the International Consortium for Atmospheric Research on Transport and Transformation 2004 campaign: Effects of size-resolved composition, J. Geophys. Res., 112, D10S31, 10.1029/2006jd007588, 2007.

Mei, F., Hayes, P. L., Ortega, A., Taylor, J. W., Allan, J. D., Gilman, J., Kuster, W., de Gouw, J., Jimenez, J. L., and Wang, J.: Droplet activation properties of organic aerosols observed at an urban site during CalNex-LA, Journal of Geophysical Research: Atmospheres, 118,

2903-2917, 10.1002/jgrd.50285, 2013.

Meier, J., Wehner, B., Massling, A., Birmili, W., Nowak, A., Gnauk, T., Brüggemann, E., Herrmann, H., Min, H., and Wiedensohler, A.: Hygroscopic growth of urban aerosol particles in Beijing (China) during wintertime: a comparison of three experimental methods, Atmos. Chem. Phys., 9, 6865-6880, 10.5194/acp-9-6865-2009, 2009.

Moore, R. H., Cerully, K., Bahreini, R., Brock, C. A., Middlebrook, A. M., and Nenes, A.: Hygroscopicity and composition of California CCN during summer 2010, Journal of Geophysical Research: Atmospheres, 117, n/a-n/a, 10.1029/2011JD017352, 2012a.

Moore, R. H., Raatikainen, T., Langridge, J. M., Bahreini, R., Brock, C. A., Holloway, J. S., Lack, D. A., Middlebrook, A. M., Perring, A. E., Schwarz, J. P., Spackman, J. R., and Nenes, A.: CCN Spectra, Hygroscopicity, and Droplet Activation Kinetics of Secondary Organic Aerosol Resulting from the 2010 Deepwater Horizon Oil Spill, Environmental Science & Technology, 46, 3093-3100, 10.1021/es203362w, 2012b.

Pöschl, U.: Atmospheric aerosols: Composition, transformation, climate and health effects, Angewandte Chemie-International Edition, 44, 7520-7541, citeulike-article-id:6549360, 2005.

Pajunoja, A., Lambe, A. T., Hakala, J., Rastak, N., Cummings, M. J., Brogan, J. F., Hao, L., Paramonov, M., Hong, J., Prisle, N. L., Malila, J., Romakkaniemi, S., Lehtinen, K. E. J., Laaksonen, A., Kulmala, M., Massoli, P., Onasch, T. B., Donahue, N. M., Riipinen, I., Davidovits, P., Worsnop, D. R., Petäjä, T., and Virtanen, A.: Adsorptive uptake of water by semisolid secondary organic aerosols, Geophysical Research Letters, 42, 3063-3068, 10.1002/2015GL063142, 2015.

Paramonov, M., Aalto, P. P., Asmi, A., Prisle, N., Kerminen, V. M., Kulmala, M., and Petäjä, T.: The analysis of size-segregated cloud condensation nuclei counter (CCNC) data and its implications for cloud droplet activation, Atmos. Chem. Phys., 13, 10285-10301, 10.5194/acp-13-10285-2013, 2013.

Park, K., Kittelson, D. B., Zachariah, M. R., and McMurry, P. H.: Measurement of inherent material density of nanoparticle agglomerates, Journal of Nanoparticle Research, 6, 267-272, 2004.

Petters, M. D., and Kreidenweis, S. M.: A single parameter representation of hygroscopic growth and cloud condensation nucleus activity, Atmos. Chem. Phys., 7, 1961-1971, 10.5194/acp-7-1961-2007, 2007.

Potukuchi, S., and Wexler, A. S.: Identifying solid-aqueous phase transitions in atmospheric aerosols—I. Neutral-acidity solutions, Atmospheric Environment, 29, 1663-1676, http://dx.doi.org/10.1016/1352-2310(95)00074-9, 1995.

Rickards, A. M. J., Miles, R. E. H., Davies, J. F., Marshall, F. H., and Reid, J. P.: Measurements of the Sensitivity of Aerosol Hygroscopicity and the κ Parameter to the O/C

Ratio, The Journal of Physical Chemistry A, 117, 14120-14131, 10.1021/jp407991n, 2013.

Sakurai, H., Fink, M. A., McMurry, P. H., Mauldin, L., Moore, K. F., Smith, J. N., and Eisele, F. L.: Hygroscopicity and volatility of 4–10 nm particles during summertime atmospheric nucleation events in urban Atlanta, Journal of Geophysical Research: Atmospheres, 110, n/a-n/a, 10.1029/2005JD005918, 2005.

Shantz, N. C., Pierce, J. R., Chang, R. Y. W., Vlasenko, A., Riipinen, I., Sjostedt, S., Slowik, J. G., Wiebe, A., Liggio, J., Abbatt, J. P. D., and Leaitch, W. R.: Cloud condensation nuclei droplet growth kinetics of ultrafine particles during anthropogenic nucleation events, Atmospheric Environment, 47, 389-398, http://dx.doi.org/10.1016/j.atmosenv.2011.10.049, 2012.

Sihto, S. L., Mikkilä, J., Vanhanen, J., Ehn, M., Liao, L., Lehtipalo, K., Aalto, P. P., Duplissy, J., Petäjä, T., Kerminen, V. M., Boy, M., and Kulmala, M.: Seasonal variation of CCN concentrations and aerosol activation properties in boreal forest, Atmos. Chem. Phys., 11, 13269-13285, 10.5194/acp-11-13269-2011, 2011.

Sloane, C. S., and Wolff, G. T.: Prediction of ambient light scattering using a physical model responsive to relative humidity: Validation with measurements from detroit, Atmospheric Environment (1967), 19, 669-680, http://dx.doi.org/10.1016/0004-6981(85)90046-0, 1985.

Stokes, R. H., and Robinson, R. A.: Interactions in Aqueous Nonelectrolyte Solutions. I. Solute-Solvent Equilibria, Journal of Physical Chemistry, 70, 2126-2130, 1966.

Suda, S. R., Petters, M. D., Yeh, G. K., Strollo, C., Matsunaga, A., Faulhaber, A., Ziemann, P. J., Prenni, A. J., Carrico, C. M., Sullivan, R. C., and Kreidenweis, S. M.: Influence of Functional Groups on Organic Aerosol Cloud Condensation Nucleus Activity, Environmental Science & Technology, 48, 10182-10190, 10.1021/es502147y, 2014.

Sun, T. L., He, L. Y., Zeng, L. W., and Huang, X. F.: Black carbon measurement during Beijing Paralympic Games, China Environmental Science, 32, 2123-2127, 2012a.

Sun, Y. L., Zhang, Q., Schwab, J. J., Yang, T., Ng, N. L., and Demerjian, K. L.: Factor analysis of combined organic and inorganic aerosol mass spectra from high resolution aerosol mass spectrometer measurements, Atmos. Chem. Phys., 12, 8537-8551, 10.5194/acp-12-8537-2012, 2012b.

Swietlicki, E., Zhou, J., Berg, O. H., Martinsson, B. G., Frank, G., Cederfelt, S.-I., Dusek, U., Berner, A., Birmili, W., Wiedensohler, A., Yuskiewicz, B., and Bower, K. N.: A closure study of sub-micrometer aerosol particle hygroscopic behaviour, Atmospheric Research, 50, 205-240, 10.1016/s0169-8095(98)00105-7, 1999.

Swietlicki, E., Hansson, H. C., HÄMeri, K., Svenningsson, B., Massling, A., McFiggans, G., McMurry, P. H., PetÄJÄ, T., Tunved, P., Gysel, M., Topping, D., Weingartner, E., Baltensperger, U., Rissler, J., Wiedensohler, A., and Kulmala, M.: Hygroscopic properties of submicrometer atmospheric aerosol particles measured with H-TDMA instruments in various

environments—a review, Tellus B, 60, 432-469, 10.1111/j.1600-0889.2008.00350.x, 2008.

Tang, I. N., and Munkelwitz, H. R.: Water activities, densities, and refractive indices of aqueous sulfates and sodium nitrate droplets of atmospheric importance, J. Geophys. Res., 99, 18801-18808, 10.1029/94jd01345, 1994.

Ulbrich, I. M., Canagaratna, M. R., Zhang, Q., Worsnop, D. R., and Jimenez, J. L.: Interpretation of organic components from Positive Matrix Factorization of aerosol mass spectrometric data, Atmos. Chem. Phys., 9, 2891-2918, 10.5194/acp-9-2891-2009, 2009.

Väkevä, M., Hämeri, K., and Aalto, P. P.: Hygroscopic properties of nucleation mode and Aitken mode particles during nucleation bursts and in background air on the west coast of Ireland, Journal of Geophysical Research: Atmospheres, 107, PAR 9-1-PAR 9-11, 10.1029/2000JD000176, 2002.

Varutbangkul, V., Brechtel, F. J., Bahreini, R., Ng, N. L., Keywood, M. D., Kroll, J. H., Flagan, R. C., Seinfeld, J. H., Lee, A., and Goldstein, A. H.: Hygroscopicity of secondary organic aerosols formed by oxidation of cycloalkenes, monoterpenes, sesquiterpenes, and related compounds, Atmos. Chem. Phys., 6, 2367-2388, 10.5194/acp-6-2367-2006, 2006.

Virkkula, A., Van Dingenen, R., Raes, F., and Hjorth, J.: Hygroscopic properties of aerosol formed by oxidation of limonene, α-pinene, and β-pinene, J. Geophys. Res., 104, 3569-3579, 10.1029/1998jd100017, 1999.

Wehner, B., Birmili, W., Ditas, F., Wu, Z., Hu, M., Liu, X., Mao, J., Sugimoto, N., and Wiedensohler, A.: Relationships between submicrometer particulate air pollution and air mass history in Beijing, China, 2004–2006, Atmos. Chem. Phys., 8, 6155-6168, 10.5194/acp-8-6155-2008, 2008.

Wong, J. P. S., Lee, A. K. Y., Slowik, J. G., Cziczo, D. J., Leaitch, W. R., Macdonald, A., and Abbatt, J. P. D.: Oxidation of ambient biogenic secondary organic aerosol by hydroxyl radicals: Effects on cloud condensation nuclei activity, Geophysical Research Letters, 38, n/a-n/a, 10.1029/2011GL049351, 2011.

Wu, Z., Hu, M., Liu, S., Wehner, B., Bauer, S., Ma ßling, A., Wiedensohler, A., Petäjä, T., Dal Maso, M., and Kulmala, M.: New particle formation in Beijing, China: Statistical analysis of a 1-year data set, Journal of Geophysical Research: Atmospheres, 112, n/a-n/a, 10.1029/2006JD007406, 2007.

Wu, Z., Hu, M., Lin, P., Liu, S., Wehner, B., and Wiedensohler, A.: Particle number size distribution in the urban atmosphere of Beijing, China, Atmospheric Environment, 42, 7967-7980, http://dx.doi.org/10.1016/j.atmosenv.2008.06.022, 2008.

Wu, Z. J., Nowak, A., Poulain, L., Herrmann, H., and Wiedensohler, A.: Hygroscopic behavior of atmospherically relevant water-soluble carboxylic salts and their influence on the water uptake of ammonium sulfate, Atmos. Chem. Phys., 11, 12617-12626, 10.5194/acp-11-12617-2011, 2011.

Wu, Z. J., Poulain, L., Henning, S., Dieckmann, K., Birmili, W., Merkel, M., van Pinxteren, D., Spindler, G., Mueller, K., Stratmann, F., Herrmann, H., and Wiedensohler, A.: Relating particle hygroscopicity and CCN activity to chemical composition during the HCCT-2010 field campaign, Atmospheric Chemistry and Physics, 13, 7983-7996, 10.5194/acp-13-7983-2013, 2013.

Wu, Z. J., Poulain, L., Birmili, W., Größ, J., Niedermeier, N., Wang, Z. B., Herrmann, H., and Wiedensohler, A.: Some insights into the condensing vapors driving new particle growth to CCN sizes on the basis of hygroscopicity measurements, Atmos. Chem. Phys. Discuss., 15, 8403-8427, 10.5194/acpd-15-8403-2015, 2015.

Ye, X., Tang, C., Yin, Z., Chen, J., Ma, Z., Kong, L., Yang, X., Gao, W., and Geng, F.: Hygroscopic growth of urban aerosol particles during the 2009 Mirage-Shanghai Campaign, Atmospheric Environment, 64, 263-269, http://dx.doi.org/10.1016/j.atmosenv.2012.09.064, 2013.

Yeung, M. C., Lee, B. P., Li, Y. J., and Chan, C. K.: Simultaneous HTDMA and HR-ToF-AMS measurements at the HKUST Supersite in Hong Kong in 2011, Journal of Geophysical Research: Atmospheres, 119, 9864-9883, 10.1002/2013JD021146, 2014.

Zdanovskii, B.: Novyi Metod Rascheta Rastvorimostei Elektrolitov v Mnogokomponentnykh Sistema, , Zh. Fiz. Khim+, 22, 1478-1485, 1486-1495, 1948.

Zhang, J., Wang, L., Chen, J., Feng, S., Shen, J., and Jiao, L.: Hygroscopicity of ambient submicron particles in urban Hangzhou, China, Front. Environ. Sci. Eng. China, 5, 342-347, 10.1007/s11783-011-0358-7, 2011.

Zheng, X., Liu, X., Zhao, F., Duan, F., Yu, T., and Cachier, H.: Seasonal characteristics of biomass burning contribution to Beijing aerosol, Science in China Ser. B Chemistry, 48, 481-488, 2005.

Table and figures

Table 1: Gravimetric densities (ρ) and hygroscopicity parameters (κ) used in this study.

Species	NH_4NO_3	NH_4HSO_4	$(NH_4)_2SO_4$	SOA	POA	BC
[kg/m^3]	1720	1780	1769	1400	1400	1700
κ	0.58	0.56	0.48	0.1	0	0

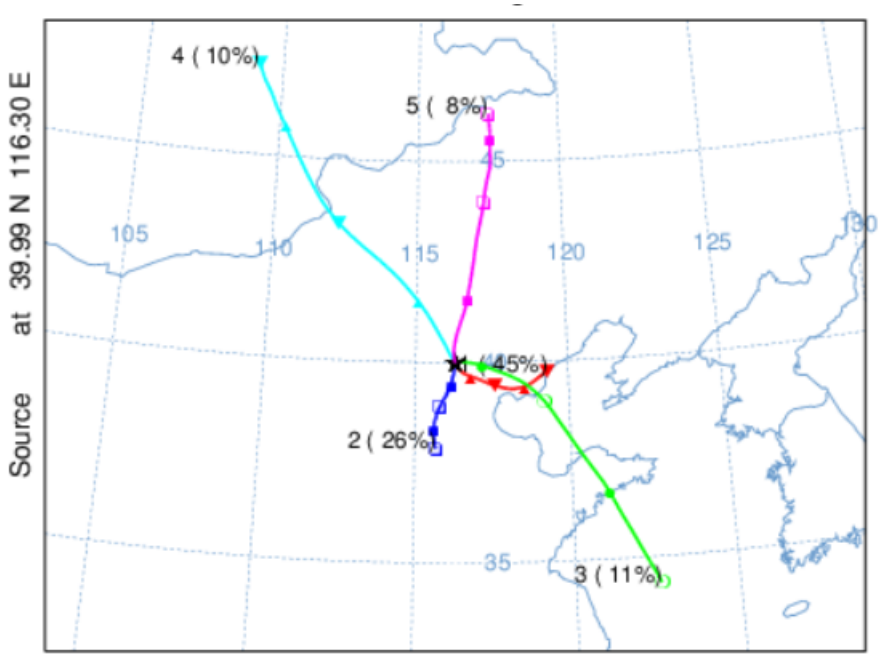

Figure 1: Mean air mass backward trajectories for five clusters arriving at the sampling site.

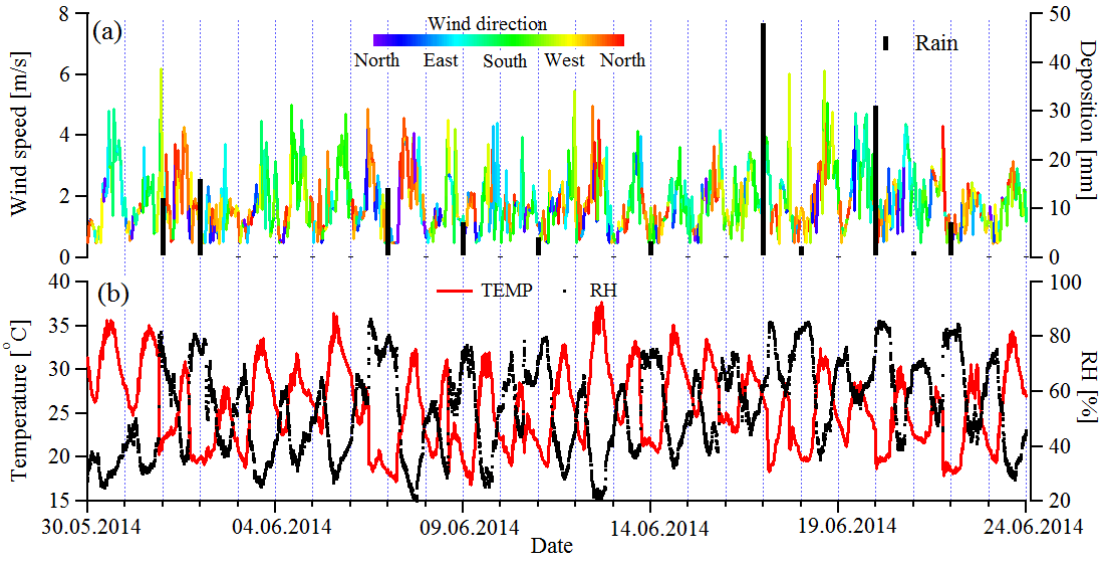

Figure 2: The time series of wind speed, wind direction, wet deposition (a) and temperature and RH (b) during the sampling period.

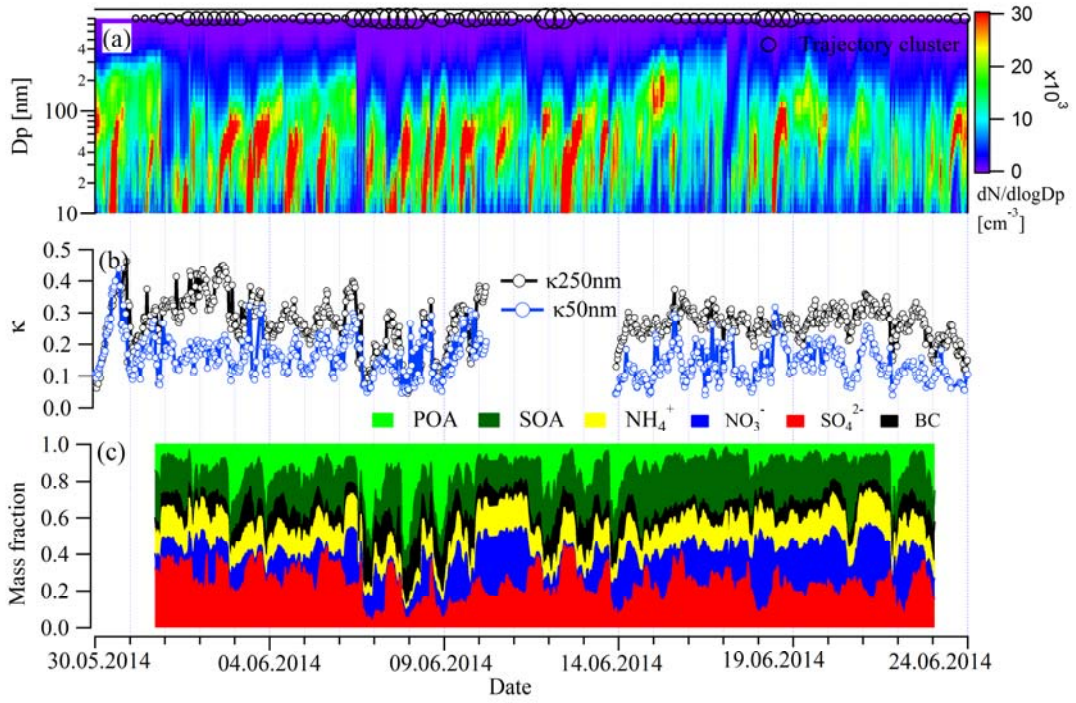

Figure 3: Time series of particle number size distribution (a), hygroscopicity parameters (κ) (b), and chemical composition of PM1 (c) during the measuring period. The black circles in the upper panel (a) indicate the trajectory clusters. The smallest circle means cluster 1, and the biggest one is cluster 5.

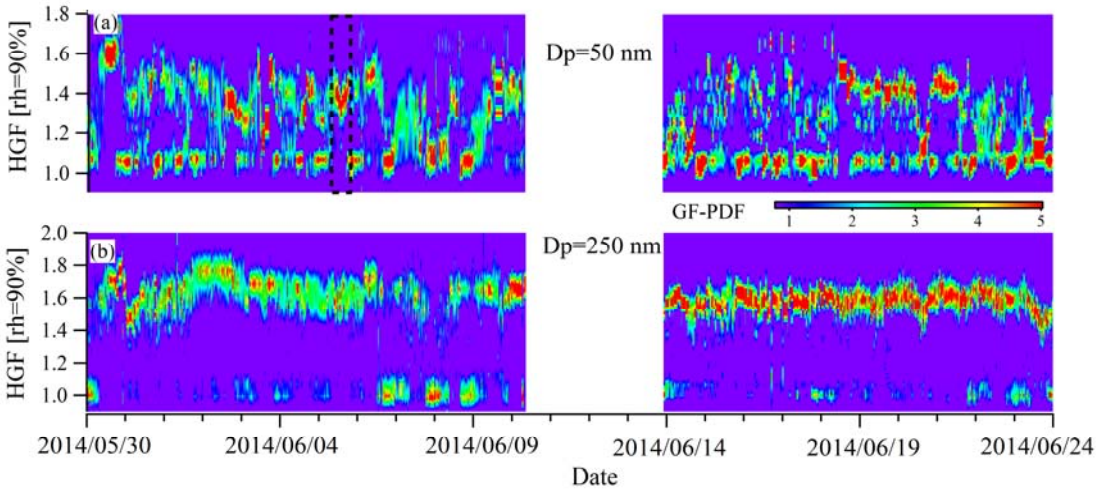

Figure 4: The time series of the GF-PDFs for 50 and 250 nm particles.

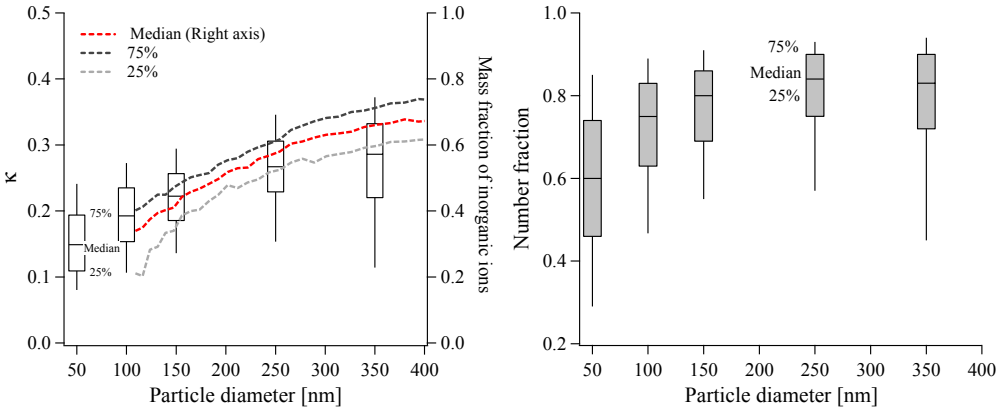

Figure 5: Size-resolved particle hygroscopicity and inorganic mass fraction (left) in NR-PM1 and Size-dependent number fraction of hydrophilic mode (right).

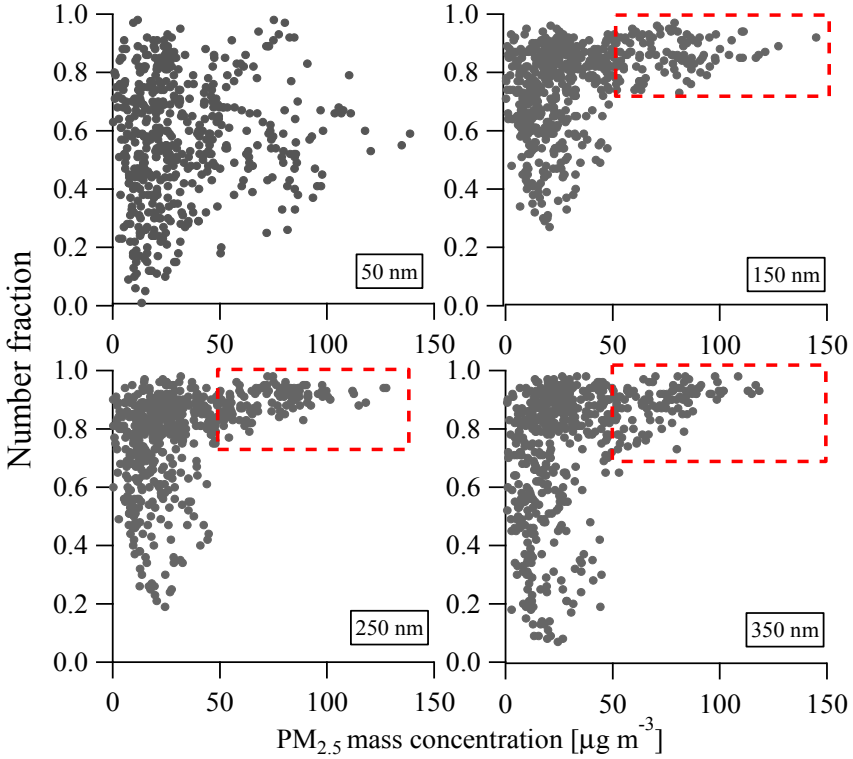

Figure 6: Number fraction of hydrophilic mode vs $PM_{2.5}$ mass concentration

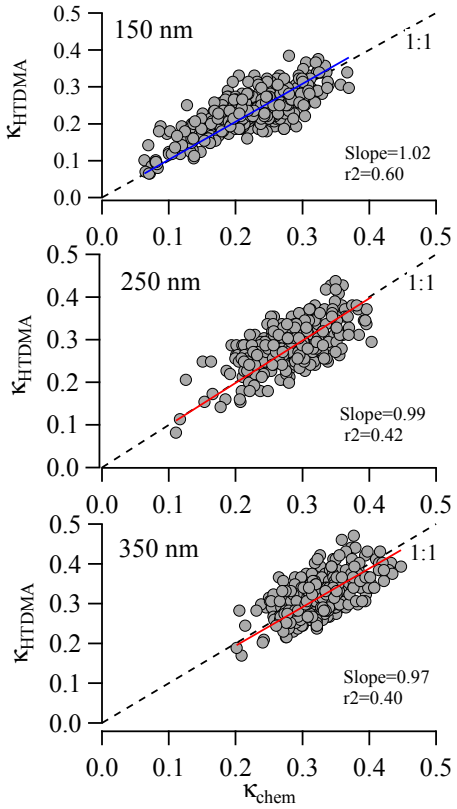

Figure 7: κ_{HTDMA} vs. κ_{chem} using size-resolved chemical composition data. All the root mean square errors (RMSE) of the linear fits were 0.04.

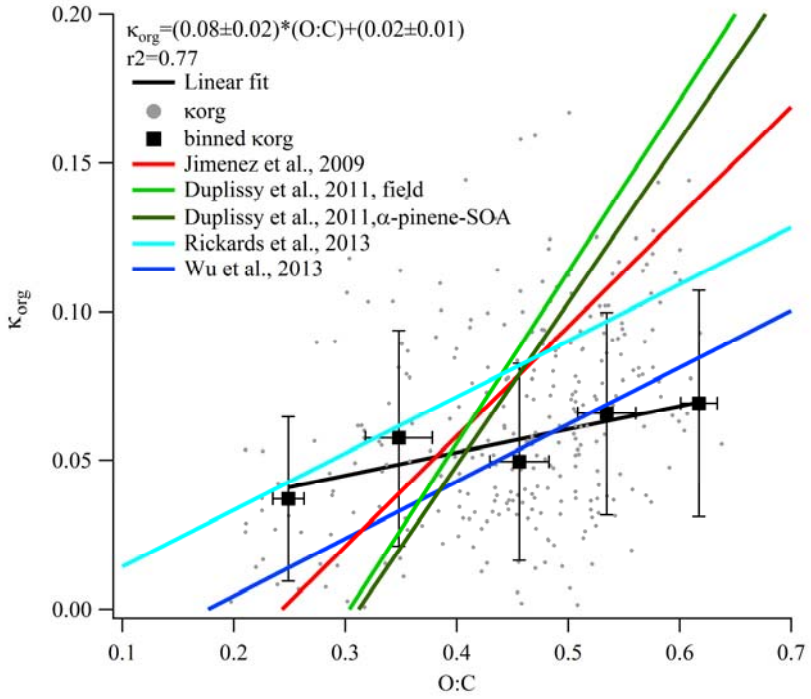

Figure 8: The relationship between organic hygroscopicity parameter (κ_{org}) and oxygen to carbon ratio (O: C).

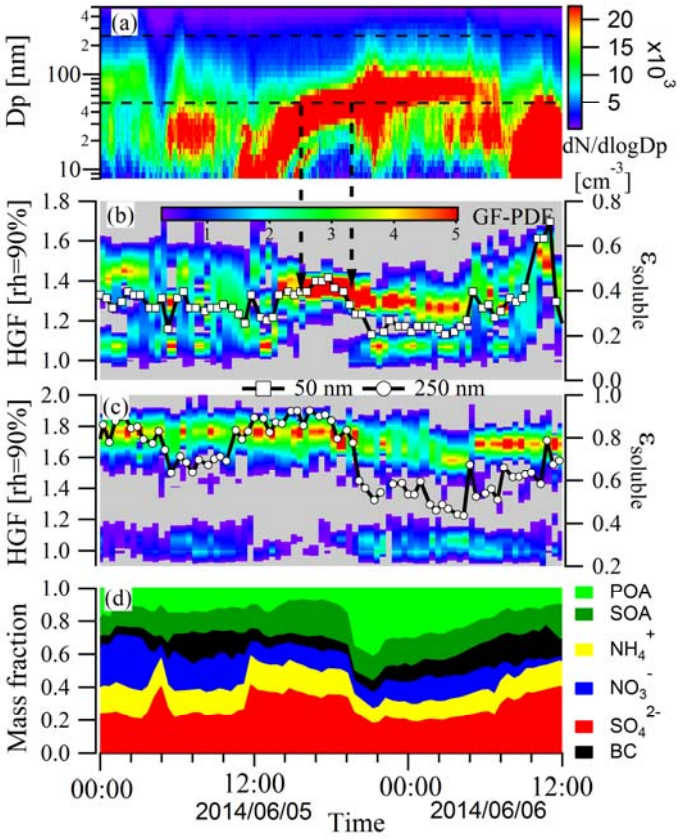

Figure 9: The variation in particle number size distribution (a), GF-PDF (b, c), water soluble volume fraction (b, c), and chemical composition of PM_1 (d) during a NPF event.